Published in final edited form as:
Biochemistry. 2013 January 22; 52(3): 477–487. doi:10.1021/bi301262p.

Structural and Mechanistic Studies of HpxO, a Novel FAD-dependent Urate Oxidase from *Klebsiella pneumoniae*†,‡

Katherine A. Hicks[§], **Seán E. O'Leary**[⊥,§], **Tadhg P. Begley**[⊥,*], and **Steven E. Ealick**[§,*]
[§]Department of Chemistry and Chemical Biology, Cornell University, Ithaca, New York 14853
[⊥]Department of Chemistry, Texas A&M University, College Station, Texas 77842

Abstract

HpxO is a flavin-dependent urate oxidase that catalyzes the hydroxylation of uric acid to 5-hydroxyisourate and functions in a novel pathway for purine catabolism found in *Klebsiella pneumoniae*. We have determined the structures of HpxO with and without uric acid at 2.0 Å and 2.2 Å, respectively. We have also determined the structure of the R204Q variant at 2.0 Å resolution in the absence of uric acid. The variant structure is very similar to wild type HpxO except for the conformation of Arg103, which interacts with FAD in the variant but not in the wild type structure. Interestingly, the R204Q variant results in the uncoupling of NADH oxidation from uric acid hydroxylation. This suggests that Arg204 facilitates the deprotonation of uric acid activating it for the oxygen transfer. Based on these data, a mechanism for this reaction is proposed consisting of a nucleophilic attack of the urate anion on the flavin hydroperoxide resulting in the formation of 5-hydroxyisourate.

The ubiquitous pathogen *Klebsiella pneumoniae* is a Gram-negative bacterium often responsible for pneumonia, wound infection and urinary tract infections in hospital and health care settings (1). *K. pneumoniae* can also be a community-acquired pathogen causing liver abscess and meningitis (2). This bacterium has developed resistance to a wide range of antibiotics including carbapenems, which are used as a last line of defense against Gram-negative infections. Within the last decade, carbapenem-resistant *K. pneumoniae* strains have been found worldwide, including Columbia, Israel and Brazil (3, 4). These resistant strains have emerged as virulent pathogens, and nosocomial infection is associated with high rates of mortality, as demonstrated in a recent, high-profile outbreak in the United States (5).

While purine catabolism is relatively well understood and many of the enzymes involved have been biochemically and structurally characterized, important problems still remain unsolved in this area of metabolite catabolism (6, 7). Recently, a 23-gene cluster involved in a novel purine catabolic pathway was identified in *K. pneumoniae* (8, 9). Putative functions

†This research was supported by a grant from the National Institutes of Health (GM073220 to SEE) and by the Robert A. Welch Foundation (A-0034 to TPB). This work is based upon research conducted at the Advanced Photon Source on the Northeastern Collaborative Access Team beamlines, which are supported by award RR-15301 from the National Center for Research Resources at the National Institutes of Health. Use of the Advanced Photon Source is supported by the U.S. Department of Energy, Office of Basic Energy Sciences, under Contract No. DE-AC02-06CH11357.

‡The Brookhaven Protein Data Bank codes for HpxO, the HpxO-Uric Acid complex and the R204Q variant are 3RP6, 3RP7, and 3RP8 respectively.

*To whom correspondence should be addressed at the Department of Chemistry and Chemical Biology, Cornell University, Ithaca, NY 14853. Telephone: (607) 255-7961. Fax: (607) 255-1227. see3@cornell.edu, begley@chem.tamu.edu.

SUPPORTING INFORMATION

The sequences of the oligomeric primers used for site-directed mutagenesis are listed in supporting information. This material is available free of charge via the Internet at http://pubs.acs.org.

have been assigned for only twelve of these gene products and include enzymes, regulators and transporters (Figure 1) (8, 9); however, many of the gene products are still biochemically and structurally uncharacterized. Interestingly, *K. pneumoniae* appears to have a complete purine catabolic pathway that continues past allantoate to provide a nitrogen source for *K. pneumoniae*; however, the enzymatic activities responsible for the latter part of the pathway have not yet been assigned (8). This pathway includes several enzymes that catalyze interesting chemical transformations, including HpxDE, a two-component oxygenase system that converts hypoxanthine to urate, HpxA, an allantoin racemase and HpxO (Figure 1).

HpxO is the enzyme responsible for the conversion of uric acid to 5-hydroxyisourate (10). This enzyme contains the sequence motif $GxGxxG(x)_{17}E$ and is therefore a member of the well-studied flavin adenine dinucleotide (FAD)-dependent glutathione reductase structural family (11). Biochemical studies indicate that HpxO belongs to the Class A flavin-dependent monooxygenase superfamily and requires FAD for activity (10, 12). These findings are in contrast to the mechanism of all other previously characterized urate oxidases, which proceed through direct reaction of an enzyme-stabilized urate dianion with triplet oxygen and do not require cofactors (13-17).

Flavin-dependent monooxygenases are well characterized (18-20). HpxO, however, is the first example of an FAD-dependent urate oxidase. In this work, we report crystal structures of the unliganded and uric acid-bound forms of HpxO from *K. pneumoniae*. Based on the liganded structure, the R204Q variant was prepared and kinetically characterized. This change results in the uncoupling of the NADH oxidation and uric acid hydroxylation reactions. The structure of the R204Q variant suggests that this residue is involved in substrate activation for oxygen transfer from the flavin hydroperoxide. Based on these data, we propose a catalytic mechanism for flavin-mediated uric acid hydroxylation.

MATERIALS AND METHODS

Cloning of K. pneumoniae HpxO

Standard methods were used for DNA manipulations (21, 22). Plasmid DNA was purified with the Fermentas GeneJet miniprep kit and DNA fragments were purified from agarose gel with the Zymoclean Gel DNA Recovery kit from Zymo Research. *E. coli* strain MachI (Invitrogen) was used as a recipient for transformations during plasmid construction and for plasmid propagation and storage. Phusion DNA polymerase (New England Biolabs) was used for PCR following the manufacturer's instructions. PfuTurbo DNA polymerase (Stratagene) was used for mutagenesis. All restriction enzymes were purchased from New England Biolabs. The plasmid THT is a derivative of pET-28, which was obtained from Novagen**,** and incorporates an N-terminal polyhistidine tag cleavable by TEV protease and a short sequence to improve solubility.

The *hpxO* gene was amplified from *Klebsiella pneumoniae* genomic DNA (ATCC catalog #: 700721D) using standard PCR conditions and the following primer pair: 5′-GGG TAG CAT ATG AAA GCA ATC GTG ATT GGC GCC-3′ and 5′-CCC TAC TCG AGT TAG CCC AGC GGC CCG CTG AGG ATG G-3′. The amplified product containing the gene was excised from the gel, purified and digested with *Nde*I and *Xho*I, repurified and ligated into similarly digested and purified pTHT. All PCR-derived DNA was sequenced to insure that the PCR process had not introduced mutations. A correct clone was named HpxO.THT and transformed into *E.coli* cell strain B834(DE3) for overexpression.

Site-Directed Mutagenesis of HpxO

Mutagenesis was performed using a standard PCR-based protocol. Colonies were screened by colony PCR with a primer specific to the mutation and either the *T7* terminator primer or the *T7* promoter primer, which binds to the plasmid backbone. The sequences of the oligomeric primers used for site-directed mutagenesis are listed in "Supporting Information."

Production of Selenomethionyl (SeMet) HpxO

Overnight cultures were grown by transferring a single colony to 15 mL of LB medium supplemented with 25 μg/mL kanamycin at 37 °C with shaking for ~16 h. The overnight cultures were pelleted by centrifugation at 4 °C for 15 min at 4,000*g*. The resulting cell pellets were resuspended in 1 L of minimal media supplemented with 1X M9 minimal salts, 20 mg/L of all amino acids except methionine, 50 mg/L L-selenomethionine, 1x MEM vitamin mix, 0.4% glucose, 2 mM $MgSO_4$, 0.1 mM $CaCl_2$, 25 mg/L $FeSO_4$ and 25 μg/mL kanamycin. Cells were grown with shaking at 37 °C. When cells reached an OD_{600} of 0.7-0.9 the temperature was lowered to 15 °C and overexpression of HpxO was induced by the addition of 1 mM isopropyl β-D-thiogalactopyranoside. After overnight growth with continued shaking (approximately ~18 h), cells were pelleted by centrifugation at 4 °C for 15 min at 6,000 *g*. Cell pellets were stored at −80 °C until purification. Cells were resuspended in ~25 mL Buffer A (20 mM Tris (pH 8), 500 mM NaCl, 30 mM imdazole, 3 mM β-mercaptoethanol) and one complete mini EDTA-free protease inhibitor cocktail tablet (Roche) was added to the resuspended cells. Cells were lysed by sonication and the cell lysate was cleared by centrifugation at 40,000*g* for 45 min at 4 °C.

SeMet HpxO was purified from the clarified cell lysate by nickel affinity chromatography. The clarified lysate was loaded onto a 3 mL column pre-equilibrated with Buffer A. The column was washed with ~40 column volumes of Buffer A and then washed with 5 column volumes of Buffer A supplemented with 50 mM imidazole. SeMet HpxO was eluted from the column by addition of 5 column volumes of Buffer A containing 250 mM imidazole. The protein was ~95% pure by SDS-PAGE analysis (results not shown). SeMet HpxO was then buffer exchanged into 10 mM Tris (pH 7.7), 30 mM NaCl and 1 mM dithiothreitol (DTT) and concentrated to 7 mg/mL as determined by Bradford assay (23). One liter of culture produced approximately 14 mg of pure SeMet HpxO.

Overexpression and Purification of the R204Q HpxO Variant

The cells were grown and purified as previously described (10) except that riboflavin (0.05 g/L) was added to the culture medium. The protein was buffer exchanged by dialysis into 0.1 M potassium phosphate (pH 8) buffer for kinetic studies. For crystallographic studies, the protein was buffer exchanged into 10 mM Tris (pH 8), 30 mM NaCl. All protein samples were purified to >90% as determined by SDS-PAGE analysis. The purified protein was concentrated to 11 mg/mL.

Crystallization of HpxO and the R204Q Variant

Initial crystallization conditions were identified using the hanging drop vapor diffusion method (Crystal Screens 1 and 2, Hampton Research; Wizard Screens 1 and 2, Emerald Biosystems) at 18 °C. Hanging drops consisted of 1.5 μL of reservoir solution and 1.5 μL of protein solution. Optimized SeMet HpxO crystals were grown in the presence of 400 μL of reservoir solution consisting of 0.05 M KH_2PO_4 and 20% PEG 8000 with 150 μL of 1:1 paraffin:silicone oil over the surface of the reservoir. The addition of the paraffin:silicone oil mixture slowed crystal growth (24) resulting in the formation of yellow needles that grew to 100–150 μm × 10-30 μm in two days. To obtain crystals of SeMet HpxO complexed with

uric acid, SeMet HpxO crystals were transferred to a drop consisting of a saturated solution of uric acid in the reservoir solution and allowed to soak for ~1.5 h at 18°C. The crystallization buffer supplemented with 30% ethylene glycerol was used as cryoprotectant. After a 5 min incubation in the cryoprotectant the sample was flash frozen in liquid nitrogen. Both SeMet HpxO and the substrate complex crystals belong to the space group $P2_12_12_1$. The asymmetric unit contains one monomer with a Matthew's number of 2.7 $Å^3$/Da and a solvent content of 54 %.

To ensure FAD binding, R204Q was incubated with 5 mM FAD at 4 °C for 2 h prior to crystallization. Drops were streak seeded using R204Q HpxO crystals grown in the absence of FAD. Crystals grew in two days at 18 °C in 0.2 M $Mg(C_2H_3O_2)_2$, 0.1 M sodium cacodylate trihydrate (pH 6.5) and 20% PEG 8000. The crystallization buffer supplemented with 30% ethylene glycol was used as the cryoprotectant. Similar to wild type HpxO, the R204Q variant belongs to the space group $P2_12_12_1$.

X-Ray Data Collection and Processing

Data were collected on a single SeMet HpxO crystal at the NE-CAT beamline 24-ID-C at the Advanced Photon Source (Argonne National Laboratory) using a Quantum315 detector (Area Detector Systems Corporation). To maximize the anomalous signal, a single wavelength anomalous diffraction experiment was conducted at the peak *f*" for selenium. Data for the SeMet HpxO crystal were collected to 2.2 Å resolution using a 1° oscillation range over 260 frames. Data for the SeMet HpxO uric acid complex were also collected to 2.0 Å resolution at beamline 24-ID-C, using a wavelength of 0.9791 Å, over 294 frames using a 1° oscillation range. Data were collected to 2.0 Å resolution for the R204Q HpxO complexed with FAD at beamline 24-ID-C, using a wavelength of 0.9792 Å, over 120 frames using a 1° oscillation range. All data were indexed, integrated and scaled using the HKL2000 suite of programs (25). Table 1 summarizes the data collection statistics.

Structure Determination, Model Building and Refinement

HpxO contains 11 methionine residues and the initial SeMet positions were located using data cut off at 2.5 Å and the program hkl2map (26, 27); 10 out of 11 SeMet residues were located. Initial electron density maps were calculated using these heavy atom sites and automated model building was performed using SHARP/autoSHARP, which succeeded in modeling 162 residues with correct side chains and 114 residues as alanine residues out of 385 total residues (28). Initial refinement was carried out using Refmac 5.0 (29) and the CCP4i interface (30). Iterative rounds of manual model building were performed with COOT (31) and later rounds of refinement were carried out using PHENIX (32). During the later rounds of refinement, water molecules were added followed by the addition of an FAD molecule. Lastly, for the substrate complex, uric acid was modeled into HpxO prior to the final round of refinement. Geometry was verified using PROCHECK (33). The refinement statistics are summarized in Table 2.

Size Exclusion Chromatography

To determine the oligomeric state of the enzyme, SeMet HpxO was analyzed using analytical size exclusion chromatography (Superdex 200 10/300 GL, GE Healthcare). The column buffer consisted of 20 mM Tris (pH 8), 50 mM NaCl and 1 DTT. Proteins of known oligomeric state were also prepared and used to generate a standard curve of partition coefficient (K_{av}) as a function of the log of the protein's molecular weight. Based on the measured K_{av} of SeMet HpxO, the protein is a monomer. All runs were performed at a flow rate of 0.5 mL/min at 4 °C.

Steady-State Kinetic Assays

For specific activity determinations, assays were carried out at 25 ± 1°C in 0.1 M potassium phosphate buffer (pH 8.0), 10 mM NADH, 2 mM uric acid and 1 mM FAD. The reaction product 5-hydroxyisourate spontaneously converts to allantoin on the time scale of the assay (10). Stock solutions were prepared freshly in this buffer on the day of the assay. Absorbance measurements were recorded on a Cary 300 Bio UV-Vis spectrophotometer (Varian). For analysis of NADH oxidation, an extinction coefficient of 0.75 mM^{-1} cm^{-1} at 385 nm was used. Protein concentrations were determined by the Bradford method (23). We previously showed that the concentrations of wild type HpxO could be determined reliably by this method (10). For purposes of calculation of V/E_o, the active protein concentration was assumed to be equal to the total protein concentration in the presence of 0.01 mM or 1 mM FAD.

For kinetics studies, the uric acid concentration was typically fixed at 1 mM in assays in which the NADH concentration was varied. When the uric acid concentration was varied, the NADH concentration was fixed at 1.5 mM. To minimize mixing effects, all other components of the HpxO reaction were typically added to the appropriate volume of NADH stock solution in order to initiate the reaction. In a typical experiment, HpxO (100–900 nM final concentration), 0–1 mM uric acid and 0.01 mM FAD were pre-incubated in 0.1 M potassium phosphate buffer, then added to an appropriate volume of 0-2 mM NADH to initiate the reaction. The reaction mixtures were then manually mixed prior to observing the absorbance change at 385 nm. The initial mixing step resulted in a delay of 12 ± 3 s between initiation of the reaction and the acquisition of the first absorbance data point. The time domain for the absorbance data at each substrate concentration was chosen to produce the best linear fit to the initial change in 385 nm absorbance.

The absorbance data were analyzed by fitting the linear portions of the initial absorbance decay by linear least-squares regression to determine the rates of change of absorbance at 385 nm as a function of initial substrate concentration. These rates were converted to rates of change of NADH concentration and plotted as a function of $[NADH]_o$. The resulting data were fit by nonlinear regression to the Michaelis-Menten equation. Regression analysis was carried out using the Grafit 5.0 software package (Erithacus Software). The kinetic constants were determined on the basis of at least two independent experiments. The standard errors reported in the text are the standard errors to the linear or nonlinear fits.

HPLC Analysis of the Products of the HpxO-catalyzed reaction

All reactions were assayed by reverse-phase HPLC on an Agilent 1100 HPLC system equipped with a quaternary pump and a 1.0 mL sample loop. The system also had a diode array UV-Vis detector (190 – 640 nm) and a fluorescence detector. The stationary phase was a Supelcosil LC–18–T column (15 cm × 4.6 mm, 3 μm particles), maintained at room temperature (21 ± 1 °C). At the end of the incubation period for the enzymatic reaction, the protein was removed by centrifugal ultrafiltration of the reaction mixture (10 kDa MWCO membrane). Aliquots of 0.02 – 0.05 mL of the filtrate were then removed and analyzed for urate and allantoin. The LC eluent consisted of a gradient of methanol in 10 mM potassium phosphate buffer (pH 6.6). In the analytical method the percentages P and M of phosphate buffer and methanol (balance water) at time t varied according to the following scheme: [t,P,M]: [0,100,0], [4,90,0], [9,60,15], [14,10,65], [16,100,0], [21,100,0].

Figure Preparation

Figures were generated using PyMOL (34) and ChemBioDraw (CambridgeSoft).

RESULTS

Structure of the HpxO Monomer

The asymmetric unit contains one monomer of HpxO and the final model contains residues 1-36 and 40-384 of the protein chain, eight residues of the polyhistidine tag spacer and one molecule of FAD. The substrate complex also contained one molecule of uric acid. A disordered region consisting of residues 37 to 39 was missing in the electron density and was therefore not included in the final model. This region is near a cavity leading to the HpxO active site. The final model is shown in Figure 2. HpxO is structurally similar to other flavin-dependent monooxygenases and consists of three domains. The N-terminal domain has a six-stranded parallel β-sheet (β7↑β2↑β1↑β11↑β18↑β17↓) flanked on one side by a three-stranded antiparallel β-sheet (β8↑β9↓β10↑) and one α-helix, and on the other side by five α-helices, a two-stranded antiparallel β-sheet (β6↓,β13↑) and a small 3_{10} helix. The N-terminal domain forms most of the interactions with the FAD molecule. The second domain consists of a seven-stranded mostly antiparallel β-sheet (β5↓β4↑β13↑β14↓β15↑β12↓β16↑) that is flanked by two α-helices that are solvent exposed. This domain forms part of the uric acid binding pocket. Finally, the C-terminal domain connects the first two domains. It consists of a long α-helix (α11) that stretches the length of HpxO and four shorter α-helices (α9, α10, α12 and α13). Based on size exclusion chromatography, HpxO is also a monomer in solution (data not shown).

FAD Binding Site

One FAD molecule binds to the HpxO monomer in an extended conformation in a cavity that is approximately 24 Å long and 9–15 Å wide. In the wild type HpxO structures obtained in the presence and absence of uric acid, the FAD is found in the *in* conformation (Figure 3) (35). Mostly hydrophobic residues surround the FAD including Ile6, Val32, Lys123, Arg124, Val125, Asp154, Gly155 and Ala159 for the adenine base and Gly7, Ala31 and Ala153 for the ribose sugar. The 2′-hydroxyl group of the ribose ring forms a hydrogen bond with the carboxylate group of Glu30 and the 3′-hydroxyl forms a water-mediated hydrogen bond to Gln107. The α-phosphate group forms a hydrogen bond to a water molecule, while the β-phosphate group interacts with the backbone amide nitrogen atom of Gly11. Other residues near this region include Gly9, Ile 10, Arg103, Gly284 and Asp285. The isoalloxazine ring is located in a binding pocket containing primarily hydrophobic residues, including Ile42, Pro292, Gly298 and Cys299. The carbonyl oxygen atom of C2 makes a hydrogen bond to the backbone amide nitrogen atom of Gly297. The N3 is hydrogen bonded to the carbonyl oxygen atoms of Ser43 and N10 forms a hydrogen bond to a water molecule.

Substrate Binding Site

To obtain the liganded complex, uric acid was soaked into SeMet HpxO by incubating the crystals for ~1.5 h at 18 °C with a reservoir solution consisting of a saturated solution of uric acid. Uric acid binds to HpxO in a pocket with an average dimension of about 10 Å. As shown in Figure 4, a channel ~6 Å wide and approximately 20 Å long, containing mainly hydrophobic and aromatic residues, allows for entry of the uric acid into the active site. The uric acid binding site and electron density are shown as Figures 5A and 5B, respectively. As shown in Figure 5A, the hydroxyl group on C6 of uric acid is 2.8 Å from the hydroxyl group at C4 of the isoalloxazine ring. The uric acid binding pocket is lined with aromatic residues, including Phe218 which forms a π-π stacking interaction with uric acid, Tyr216, which forms a hydrogen bond to the oxygen atom on C8 of uric acid, Tyr 195, Tyr216, Phe218, Trp45 and Trp195. A number of charged residues are also found in the active site, including most notably Arg204, which forms hydrogen bonds with both the amide nitrogen (N3) and oxygen at the urate C2. Other charged residues in the uric acid binding pocket are Asn178,

Asp220 and Asp293. A number of nonpolar amino acid residues, including Met208, Pro292, Ile294 and Gly295, are also located in the uric acid binding pocket.

R204Q HpxO Variant Structure

Due to the significant effect of the R204Q variant on catalysis (Table 3), crystals of HpxO containing the R204Q variant were obtained in the presence of FAD. The asymmetric unit contains one monomer of R204Q HpxO and the final model contains residues 1-35 and 40-384 of the protein chain, one residue of the His_6 tag and one molecule of FAD. Residues 36 to 39 form a flexible loop region, which is missing from the electron density, and thus is not included in the final model. The overall fold of the R204Q HpxO is the same as the wild type (Figure 2) and also consists of three domains. One FAD molecule binds to the R204Q HpxO monomer in an extended conformation. As shown in Figure 6, the FAD adopts the *in* conformation in the R204Q structure. FAD is also in the *in* conformation in the wild type HpxO structures determined in the presence or absence of uric acid (Figure 3). Attempts to crystallize the HpxO(R204Q)/uric acid/FAD complex produced crystals that diffracted to >6 Å resolution and decayed rapidly due to radiation damage, thus preventing structural analysis. The residues in the FAD binding site in R204Q adopt the same conformation as in the wild type binding site, with the exception of Arg103 (Figures 3 and 6).

Steady-state kinetic analysis

To interrogate the roles of R204 and Y216 in catalysis, the steady-state kinetics of NADH oxidation were measured for the HpxO R204Q and Y216F variants (Table 3). The R204Q mutant catalyzed slow oxidation of NADH with a rate that was unaltered by the presence of urate (k_{cat} ~ 0.25 s^{-1}); this rate is comparable with that of the wild type enzyme in the absence of urate. Low levels of allantoin formation could be observed upon extended incubation of HpxO R204Q with urate and NADH in the presence of FAD, but the rate and extent of this reaction were too low to allow construction of a Michaelis-Menten plot for urate. The $K_{m\ (NADH)}$ for NADH oxidation catalyzed by HpxO R204Q was increased slightly in comparison with the wild type enzyme (640 *vs.* 500 μM). The ~10^4-fold reduction in $k_{cat}/K_{m\ (NADH)}$ is entirely a consequence of the reduced k_{cat} value.

In contrast, the Y216F variant exhibited measurable but significantly reduced activity ($k_{cat}/K_{m\ (urate)}$ ~10% of wild type enzyme). The K_m for urate was doubled, while the K_m for NADH was decreased five-fold relative to the wild type enzyme, to 100 μM for HpxO Y216F. Thus while $k_{cat}/K_{m\ (urate)}$ is an order of magnitude lower for this variant compared with the wild type enzyme, $k_{cat}/K_{m\ (NADH)}$ is essentially unchanged, dropping to 0.084 $\mu M^{-1}\ s^{-1}$ from 0.125 $\mu M^{-1}\ s^{-1}$.

DISCUSSION

Comparison of HpxO to Other Enzymes

Recent biochemical characterization confirmed that HpxO is a member of the flavin monooxygenase family and requires one molecule of FAD for optimal activity (10). Based on analysis using the DALI structure server (36), the five closest structural homologues to HpxO are listed in Table 4. These enzymes are 2,6-dihydroxypyridine 3-hydroxylase (DHPH), MHPCO, PHBH, phenol hydroxylase and 3-hydroxybenzoate hydrolase (MHBH). The rmsd for each of these enzymes to HpxO is less than 3.2 Å for at least 360 aligned residues with Z-scores of 21.0 or higher. A flavin-dependent monooxygenase similar to HpxO, but involved in the metabolism of caffeine by *Pseudomonas* sp. strain CBB1 was recently identified; this enzyme catalyzes the conversion of 1,3,7-trimethyluric acid to 1,3,7-trimethyl-5-hydroxyisouric acid but differs in its substrate binding pocket and does not catalyze monooxygenation of uric acid (37).

The FAD binding site is well-conserved among members of the Class A flavin monooxygenase superfamily (12, 35, 38-41). In HpxO the adenine ring of FAD is bound between an arginine residue (Arg124) and an aspartate residue (Asp154). Conserved residues in the FAD binding pocket include Glu30, which is oriented towards the hydroxyl groups of the ribose ring, and Gly7, Gly11 and Asp285 (39, 40). Based on previous structural studies of other flavin monooxygenases, including most notably PHBH and RebC, the isoalloxazine ring of FAD adopts three main conformations: *in*, *open* and *out*. During the catalytic reaction, FAD reduction by NADH occurs in the "out" site and hydroperoxyflavin-mediated substrate hydroxylation occurs in the "in" site (35, 42, 43). In the "open" conformation, the flavin occupies the "in" site, but the substrate is not bound. The conformation change from "*in*" to "*out*" requires ~7-8 Å of FAD movement and is usually enhanced by substrate binding. In all HpxO structures obtained (liganded, unliganded and R204Q), the FAD molecule binds lengthwise in an extended conformation with the isoalloxazine ring adopting the *in* conformation (Figures 3 and 6).

The NADH binding site is also well conserved among members of the Class A flavin monooxygenase superfamily (12). The NADH binding site has not been identified in HpxO; however, structural alignment of the HpxO/uric acid complex with R220Q PHBH (PDB ID 1K0J) (44) identifies a groove near the surface of HpxO where NADH could bind. However, the distance between the C4 on the nicotinamide ring is ~20 Å from the N5 of the flavin suggesting that for reduction of the flavin to take place there must be movement of the flavin to the *out* conformation and also movement of the NADH (44). This movement would ensure that FAD reduction occurs on the *re* face of the isoalloxazine ring (35). However, similar to MHPCO, the FAD conformation in HpxO is in the *in* conformation irrespective of the presence or absence of substrate (40). Manual modeling of the flavin C4a-hydroperoxide intermediate into the HpxO active site indicates that the terminal oxygen of the hydroperoxide intermediate is approximately 3.4 Å from the C5 of uric acid (data not shown), indicating that the substrate and cofactor are well-positioned to react.

The mechanism of substrate binding differs widely for the flavin monooxygenases (39-41). HpxO contains a tunnel, mainly comprised of hydrophobic and aromatic residues, which we hypothesize allows for uric acid binding (Figure 4). The opening to this tunnel is a disordered loop region (residues 37-39), which was not present in the HpxO electron density. It appears that this loop region could control tunnel access. The loop remains disordered in the HpxO/uric acid complex, consistent with the idea that assembly of the HpxO·FAD·urate·NADH complex is required prior to closure of the active site. This region aligns with a similar flexible loop in phenol hydroxylase (PDB ID: 1FOH). In the phenol hydroxylase reaction, this loop moves during catalysis to accommodate changes in FAD conformation (38).

As shown in Figure 5A, the active site of HpxO contains aromatic, nonpolar and charged residues. The aromatic residues include Trp45, Tyr195, Tyr216 and Phe218. The high number of aromatic residues in the HpxO active site is not surprising, as other flavin monooxygenases also contain many aromatic residues, some of which are involved in **π-π** stacking interactions (45). The nonpolar residues in the HpxO active site are Met208, Pro292, Ile294 and Gly295 and the charged residues include Asn178, Arg204, Asp220 and Asp293. Another common feature of the active sites of flavin monooxygenases is a conserved proline residue above the FAD isoalloxazine ring; this residue is Pro292 in HpxO.

The majority of the interactions between HpxO and uric acid involve interactions with Arg204, which forms two hydrogen bonds with uric acid. Specifically, the guanidium group of Arg204 forms hydrogen bonds with both O2 and N3 of the uric acid. The other interaction between HpxO and uric acid is the hydrogen bond between the hydroxyl group

of Tyr216 and O8 of uric acid. These interactions are important for both proper substrate orientation and catalysis (see below).

Comparison of Wild Type and R204Q HpxO Structures

The conformation of the residues in the FAD binding site of HpxO are largely identical in the wild type and R204Q structures with the exception of Arg103, which moves approximately 3.4 Å between the two structures (Figure 6). In the R204Q structure, the guanidinium group on Arg103 is pointed directly towards the hydroxyl groups on the ribityl side chain of FAD and forms a salt bridge to the hydroxyl groups on carbons 2 and 4. In the wild type structure, the guanidinium group of Arg103 is pointed away from the FAD and the distance between the guanidinium group and the hydroxyl on carbon 2 is more than 6 Å. However, we can not rule out that the altered conformation of Arg103 could be caused by differences in the crystallization conditions of the wild type enzyme versus the R204Q variant. Minor changes are also seen in the conformation of Asn178.

The conformations of the residues in the uric acid binding site are similar in the wild type and R204Q HpxO structures. The most significant change is in the position of Tyr216, which in the R204Q structure resides closer to the uric acid binding pocket by approximately ~1.9 Å (Figure 6). Minor changes in the position of Met208 and Pro292 are also observed.

Uncoupled NADH Oxidation with HpxO R204Q

The purified R204Q variant exhibited lower FAD occupancy than wild type HpxO but could be quantitatively reconstituted by incubation with 0.01 mM FAD. The excess cofactor could then be removed by gel filtration.

Steady-state kinetic studies on HpxO R204Q indicated that the presence of uric acid had no effect on the steady state kinetics of oxidation of NADH. The K_m value for NADH was close to the value for the wild type enzyme in the presence of saturating concentrations of urate and the k_{cat} value was 160 times slower than the wild type enzyme.

Mechanistic Implications

A mechanistic proposal for the HpxO-catalyzed oxidation of uric acid by the flavin hydroperoxide is shown in Figure 7. Structure **11** shows the interactions between the enzyme and the uric acid substrate. Arg204 deprotonates N3 of the substrate and stabilizes the resulting anion by hydrogen bonding to the C2 carbonyl. A similarly-positioned and highly conserved arginine residue is observed in the crystal structure of cofactor-independent urate oxidase bound to a urate analogue (46) where urate deprotonation to form the dianion is critical for substrate activation. In addition to forming hydrogen bonds with urate, Arg204 forms a hydrogen bond to Asp220, which in turn hydrogen bonds to His348. Asp293 bridges His 348 and Tyr176 and a water molecule joins Tyr176 and Arg204. This unusual hydrogen bonding network is otherwise mostly buried in a hydrophobic region near the active site and may be responsible for lowering the pKa of Arg204. An active site water is hydrogen bonded to N9 and Tyr216 is hydrogen bonded to the C8 carbonyl anchoring the substrate in the active site. The negative charge on N3 is delocalized onto C5, enhancing the nucleophilicity of this carbon for attack on the flavin hydroperoxide **10** to give **12** and **13**. Product dissociation and loss of water from the hydroxyflavin **12** completes the formation of 5-hydroxyisourate **3** which spontaneously converts to allontoin **6** under the assay conditions (10). Active site mutagenesis studies are consistent with the proposed roles for Arg204 and Tyr216 (Table 3). The Y216F variant shows small effects on catalysis consistent with a role in substrate binding rather than N9 deprotonation. In contrast, k_{cat} for the R204Q variant was 160-fold lower than wild type HpxO in k_{cat} while $K_{m\ (NADH)}$ increased slightly,

consistent with an important function in substrate activation by deprotonation. In addition, the NADH oxidase activity of the R204Q variant was independent of added uric acid, and comparable with wild type NADH oxidase activity in the absence of urate, suggesting that without substrate deprotonation, oxygen transfer does not occur efficiently. A small amount of allantoin could be detected after extended incubation of the R204Q variant with urate and NADH, consistent with the proposal that the variant enzyme can catalyze both NADH oxidation and urate hydroxylation, but that the coupling between the two reactions is eliminated.

In summary, our structural and biochemical characterizations of HpxO provide new mechanistic insights into the first example of an FAD-dependent urate oxidase and suggest a new mechanism for the conversion of urate to 5-hydroxyisourate.

Supplementary Material

Refer to Web version on PubMed Central for supplementary material.

Acknowledgments

The authors wish to thank the staff scientists at the APS NE-CAT beamlines for their assistance in data collection. Dr. Cynthia Kinsland of the Cornell Protein Production facility is thanked for providing clones of HpxO and the variant enzymes. We also thank members of the Ealick laboratory for comments on and editing of the manuscript. Dr. Yang Zhang is acknowledged and thanked for helpful discussions about this work. Leslie Kinsland's assistance during manuscript preparation is greatly appreciated.

ABBREVIATIONS

FAD	flavin adenine dinucleotide
SeMet	selenomethionyl
Tris	tris(hydroxymethyl)aminomethane base
DTT	dithiothreitol
UA	uric acid
DHPH	2,6-dihydroxypyridine 3-hydroxylase
MHPCO	2-methyl-3-hydroxypyridine-5-carboxylic acid oxygenase
PHBH	*p*-hydroxybenzoate hydroxylase
MHBH	3-hydroxybenzoate hydrolase
DHP	2,6-dihydroxypyridine

REFERENCES

1. Vanwynsberghe T, Verhamme K, Raymaekers M, Cartuyvels R, Van Vaerenbergh K, Boel A, de Beenhouwer H. A Large Hospital Outbreak of *Klebsiella pneumoniae* (DHA-1 and SHV-11 Positive): Importance of Detection and Treatment of ampC-Lactamases. The Open Infectious Diseases J. 2009; 3:55–60.
2. Ko W-C, Paterson DL, Sagnimeni AJ, Hansen DS, Von Gottberg A, Mohapatra S, Casellas JM, Goossens H, Mulazimoglu L, Trenholme G, Klugman KP, McCormack JG, Yu VL. Community-Acquired *Klebsiella pneumoniae* Bacteremia: Global Differences in Clinical Patterns. Emerging Infectious Diseases. 2002; 8:160–166. [PubMed: 11897067]
3. Maltezou HC. Metallo-β-lactamases in Gram-negative bacteria: introducing the era of pan-resistance? Int. J. Antimicrobial Agents. 2009; β33:405.e401–405.e407.

4. Nordmann P, Cuzon G, Naas T. The real threat of *Klebsiella pneumoniae* carbapenemase-producing bacteria. The Lancet. 2009; 9:228–236.
5. Snitkin Evan S, Zelazny Adrian M, Thomas Pamela J, Stock F, Henderson David K, Palmore Tara N, Segre Julia A. Tracking a Hospital Outbreak of Carbapenem-Resistant Klebsiella pneumoniae with Whole-Genome Sequencing. Science translational medicine. 2012; 4:148ra116.
6. Zrenner R, Stitt M, Sonnewald U, Boldt R. Pyrimidine and Purine Biosynthesis and Degradation in Plants. Annual Review of Plant Biology. 2006; 57:805–836.
7. Vogels GD, Van der Drift C. Degradation of purines and pyrimidines by microorganisms. Bacteriol Rev. 1976; 40:403–468. [PubMed: 786256]
8. de la Riva L, Badia J, Aguilar J, Bender RA, Baldoma L. The hpx Genetic System for Hypoxanthine Assimilation as a Nitrogen Source in Klebsiella pneumoniae: Gene Organization and Transcriptional Regulation. J. Bacteriol. 2008; 190:7892–7903. [PubMed: 18849434]
9. Pope SD, Chen L-L, Stewart V. Purine Utilization by *Klebsiella oxytoca* M5al: Genes for Ring-Oxidizing and -Opening Enzymes. J. Bacteriol. 2009; 191:1006–1017. [PubMed: 19060149]
10. O'Leary SE, Hicks KA, Ealick SE, Begley TP. Biochemical Characterization of the HpxO Enzyme from *Klebsiella pneumoniae*, a Novel FAD-Dependent Urate Oxidase. Biochemistry. 2009; 48:3033–3035. [PubMed: 19260710]
11. Dym O, Eisenberg D. Sequence-structure analysis of FAD-containing proteins. Protein Sci. 2001; 10:1712–1728. [PubMed: 11514662]
12. van Berkel WJH, Kamerbeek NM, Fraaije MW. Flavoprotein monooxygenases, a diverse class of oxidative biocatalysts. J. Biotechnol. 2006; 124:670–689. [PubMed: 16712999]
13. Busi E, Terzuoli L, Basosi R, Porcelli B, Marinello E. EPR Spin Trapping of a Radical Intermediate in the Urate Oxidase Reaction. Nucleosides, Nucleotides & Nucleic Acids. 2004; 23:1131–1134.
14. Kahn K, Tipton PA. Kinetic Mechanism and Cofactor Content of Soybean Root Nodule Urate Oxidase. Biochemistry. 1997; 36:4731–4738. [PubMed: 9125493]
15. Tipton PA. Urate oxidase: single-turnover stopped-flow techniques for detecting two discrete enzyme-bound intermediates. Methods in Enzymology. 2002; 354:310–319. [PubMed: 12418236]
16. Imhoff RD, Power NP, Borrok MJ, Tipton PA. General Base Catalysis in the Urate Oxidase Reaction: Evidence for a Novel Thr-Lys Catalytic Diad. Biochemistry. 2003; 42:4094–4100. [PubMed: 12680763]
17. Sarma AD, Tipton PA. Evidence for Urate Hydroperoxide as an Intermediate in the Urate Oxidase Reaction. Journal of the American Chemical Society. 2000; 122:11252–11253.
18. Harayama S, Kok M, Neidle EL. Functional and Evolutionary Relationships Among Diverse Oxygenases. Annu. Rev. Microbiol. 1992; 46:565–601. [PubMed: 1444267]
19. Torres Pazmino DE, Winkler M, Glieder A, Fraaije MW. Monooxygenases as biocatalysts: Classification, mechanistic aspects and biotechnological applications. J. Biotechnol. 2010; 146:9–24. [PubMed: 20132846]
20. Fagan, RL.; Palfey, BA. 7.03 - Flavin-Dependent Enzymes. In: Lew, M.; Hung-Wen, L., editors. Comprehensive Natural Products II. Elsevier; Oxford: 2010. p. 37-113.
21. Ausubel, FM.; Brent, R.; Kingston, RE.; Moore, DD,G,S.; Smith, JA.; Struhl, K. Short Protocols in Molecular Biology. 5th Edition. John Wiley and Sons; Chichester, UK: 2002.
22. Maniatis, T.; Fritsch, EF.; Sambrook, J. Molecular Cloning: A Laboratory Manual. Cold Spring Harbor Laboratory; Cold Spring Harbor, NY: 1982.
23. Bradford MM. A rapid and sensitive method for the quantitation of microgram quantities of protein utilizing the principle of protein-dye binding. Anal. Biochem. 1976; 72:248–254. [PubMed: 942051]
24. Chayen N. A novel technique to control the rate of vapour diffusion, giving larger protein crystals. Journal of Applied Crystallography. 1997; 30:198–202.
25. Otwinowski, Z.; Minor, W.; Charles, W.; Carter. Methods in Enzymology. Academic Press; 1997. Processing of X-ray diffraction data collected in oscillation mode; p. 307-326.
26. Pape T, Schneider TR. HKL2MAP: a graphical user interface for phasing with SHELX programs. J. App. Crystallogr. 2004; 37:843–844.

27. Schneider TR, Sheldrick GM. Substructure solution with SHELXD. Acta Crystallogr. D. 2002; 58:1772–1779. [PubMed: 12351820]
28. Vonrhein C, Blanc E, Roversi P, Bricogne G. Automated structure solution with autoSHARP. Methods Molec. Biol. 2007; 364:215–230. [PubMed: 17172768]
29. Murshudov GN, Vagin AA, Lebedev A, Wilson KS, Dodson EJ. Efficient anisotropic refinement of macromolecular structures using FFT. Acta Crystallogr. D. 1999; 55:247–255. [PubMed: 10089417]
30. Collaborative Computational Project-Number 4. The CCP-4 suite: programs for protein crystallography. Acta. Crystallogr. D. 1994; 50:760–763. [PubMed: 15299374]
31. Emsley P, Cowtan K. Coot: model-building tools for molecular graphics. Acta Crystallogr. D. 2004; 60:2126–2132. [PubMed: 15572765]
32. Adams PD, Afonine PV, Bunkoczi G, Chen VB, Davis IW, Echols N, Headd JJ, Hung L-W, Kapral GJ, Grosse-Kunstleve RW, McCoy AJ, Moriarty NW, Oeffner R, Read RJ, Richardson DC, Richardson JS, Terwilliger TC, Zwart PH. PHENIX: a comprehensive Python-based system for macromolecular structure solution. Acta Crystallogr. D. 2002; 66:213–221. [PubMed: 20124702]
33. Laskowski RA, MacArthur MW, Moss DS, Thornton JM. PROCHECK: a program to check the stereochemical quality of protein structures. J. Appl. Crystallogr. 1993; 26:283–291.
34. DeLano, WL. The PyMOL Molecular Graphics System. DeLano Scientific; San Carlos, CA: 2002.
35. Cole LJ, Entsch B, Ortiz-Maldonado M, Ballou DP. Properties of *p*-Hydroxybenzoate Hydroxylase When Stabilized in Its Open Conformation. Biochemistry. 2005; 44:14807–14817. [PubMed: 16274228]
36. Holm L, Rosenstrom P. Dali server: conservation mapping in 3D. Nucleic Acids Res. 2010; 38:W545–549. [PubMed: 20457744]
37. Mohanty SK, Yu C-L, Das S, Louie TM, Gakhar L, Subramanian M. Delineation of the caffeine C-8 oxidation pathway in Pseudomonas sp. strain CBB1 via characterization of a new trimethyluric acid monooxygenase and genes involved in trimethyluric acid metabolism. J. Bacteriol. 2012; 194:3872–3882. [PubMed: 22609920]
38. Enroth C, Neujahr H, Schneider G, Lindqvist Y. The crystal structure of phenol hydroxylase in complex with FAD and phenol provides evidence for a concerted conformational change in the enzyme and its cofactor during catalysis. Structure. 1998; 6:605–617. [PubMed: 9634698]
39. Hiromoto T, Fujiwara S, Hosokawa K, Yamaguchi H. Crystal Structure of 3-Hydroxybenzoate Hydroxylase from *Comamonas testosteroni* Has a Large Tunnel for Substrate and Oxygen Access to the Active Site. J. Mol. Biol. 2006; 364:878–896. [PubMed: 17045293]
40. McCulloch KM, Mukherjee T, Begley TP, Ealick SE. Structure of the PLP Degradative Enzyme 2-Methyl-3-hydroxypyridine-5-carboxylic Acid Oxygenase from *Mesorhizobium loti* MAFF303099 and Its Mechanistic Implications. Biochemistry. 2009; 48:4139–4149. [PubMed: 19317437]
41. Treiber N, Schulz GE. Structure of 2,6-Dihydroxypyridine 3-hydroxylase from a Nicotine-degrading Pathway. J. Mol. Biol. 2008; 379:94–104. [PubMed: 18440023]
42. Cole LJ, Gatti DL, Entsch B, Ballou DP. Removal of a Methyl Group Causes Global Changes in *p*-Hydroxybenzoate Hydroxylase. Biochemistry. 2005; 44:8047–8058. [PubMed: 15924424]
43. Ryan KS, Chakraborty S, Howard-Jones AR, Walsh CT, Ballou DP, Drennan CL. The FAD Cofactor of RebC Shifts to an IN Conformation upon Flavin Reduction. Biochemistry. 2008; 47:13506–13513. [PubMed: 19035832]
44. Wang J, Ortiz-Maldonado M, Entsch B, Massey V, Ballou D, Gatti DL. Protein and ligand dynamics in 4-hydroxybenzoate hydroxylase. Proc. Natl. Acad. Sci. USA. 2002; 99:608–613. [PubMed: 11805318]
45. Entsch B, van Berkel WJ. Structure and mechanism of para-hydroxybenzoate hydroxylase. FASEB J. 1995; 9:476–483. [PubMed: 7737455]
46. Retailleau P, Colloch N, Vivares D, Bonnete F, Castro B, El Hajji M, Mornon J-P, Monard G, Prange T. Complexed and ligand-free high-resolution structures of urate oxidase (Uox) from *Aspergillus flavus*: a reassignment of the active-site binding mode. Acta Crystallogr. D. 2004; 60:453–462. [PubMed: 14993669]

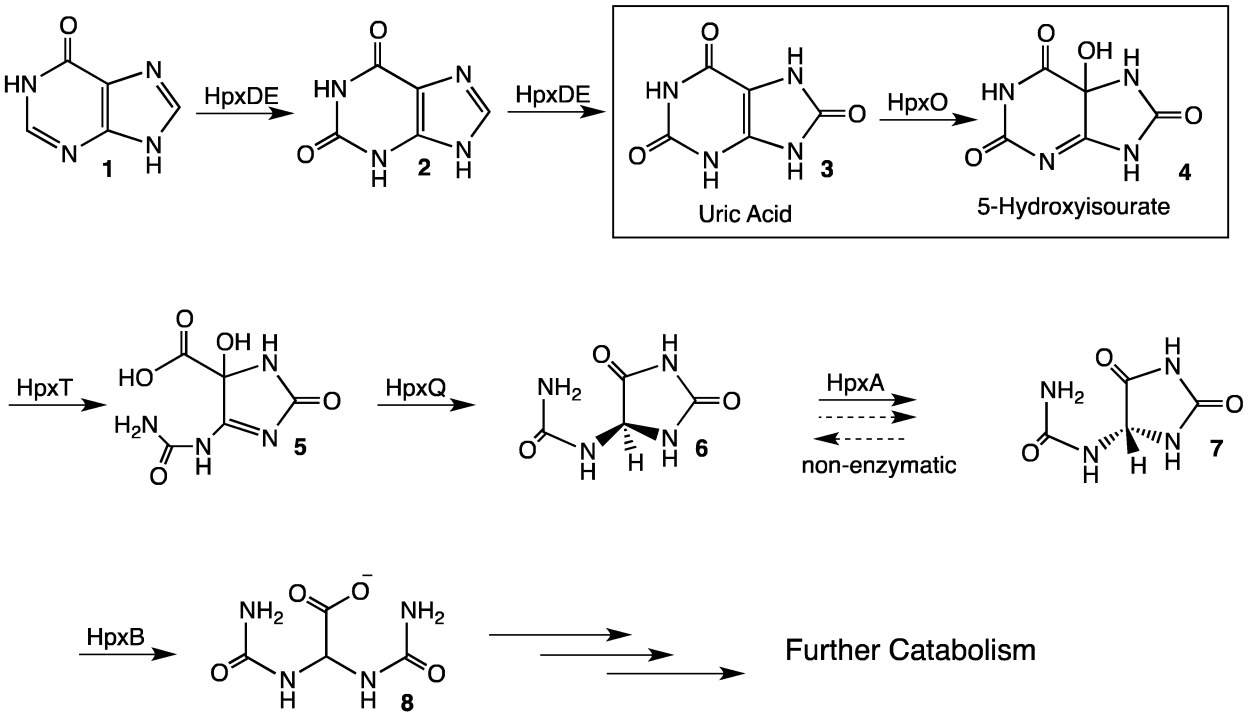

Figure 1.
The purine degradation pathway in *K. pneumoniae*.

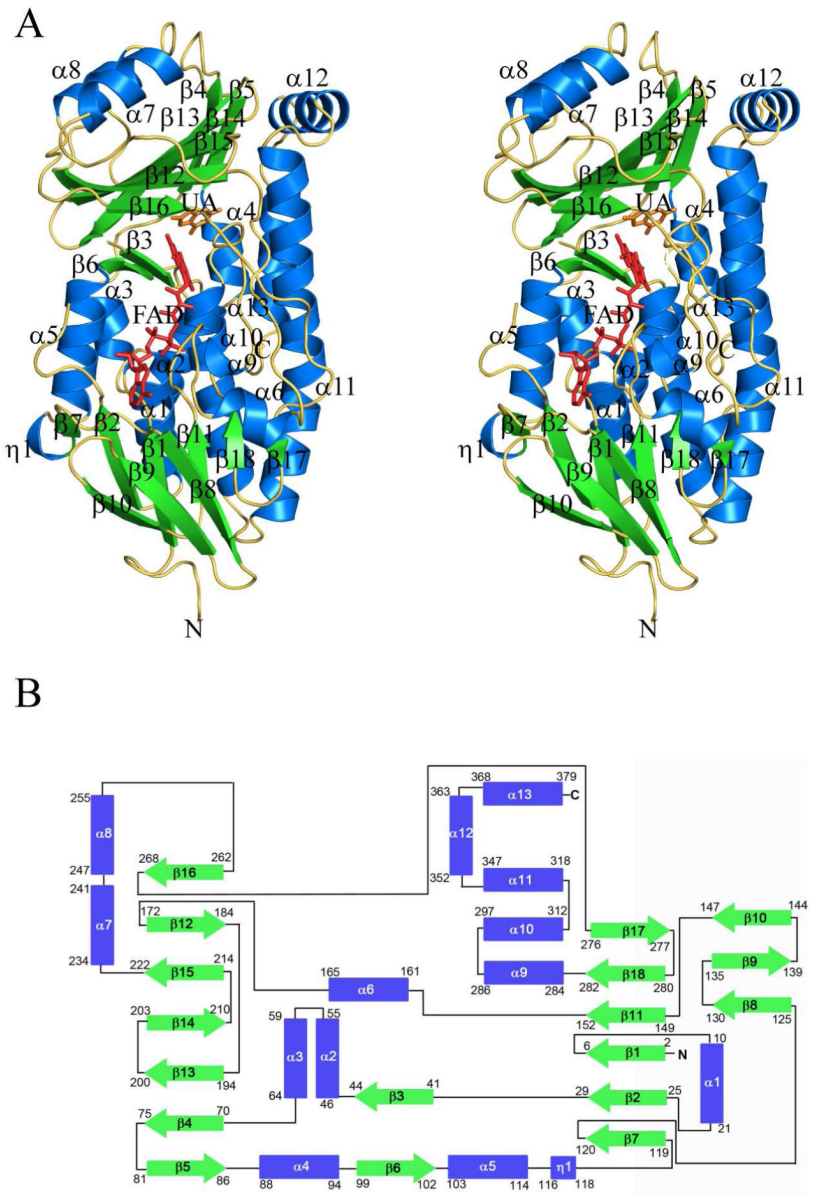

Figure 2.

Structure of HpxO. (A) Stereoview ribbon diagram of HpxO with FAD and uric acid bound and secondary structural elements labeled. The α-helices are shown in blue and the β-strands are shown in green with loops colored yellow. Ligands are shown in stick representation: FAD is colored red and uric acid is labeled as “UA” and is colored orange. (B) Topology diagram of HpxO. The color scheme is the same as Figure 2A.

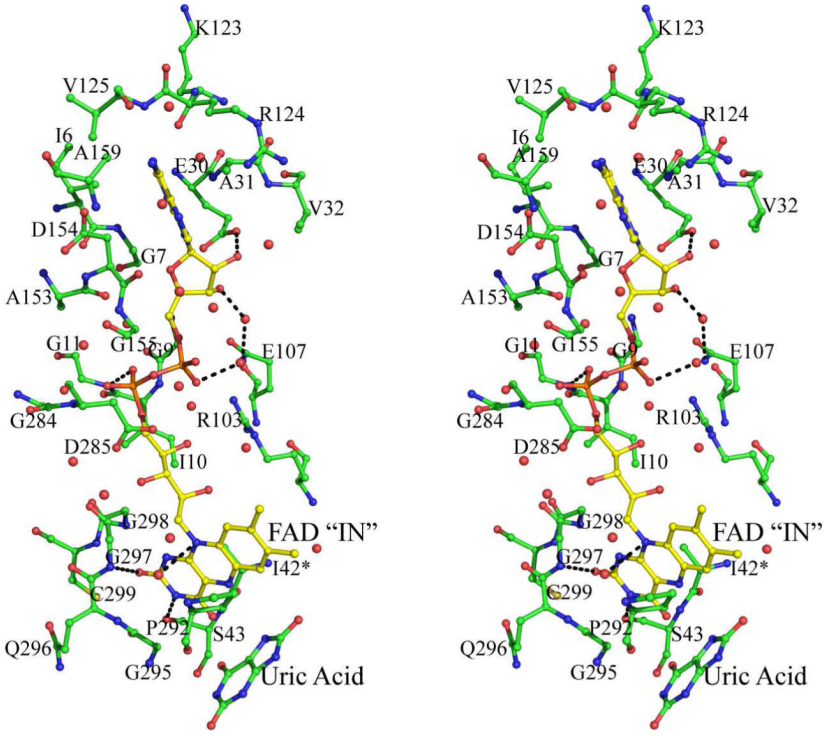

Figure 3.

Stereoview diagram of FAD binding site in HpxO with uric acid bound. The carbon residues in HpxO and uric acid are shown in green using the ball and stick representation and the interactions with the protein indicated using black dashed lines. Water molecules are shown as red nonbonded spheres. FAD adopts the *in* conformation and is shown with yellow carbon atoms. Clear electron density is not seen for the side chain of Ile42, which labeled as I42*.

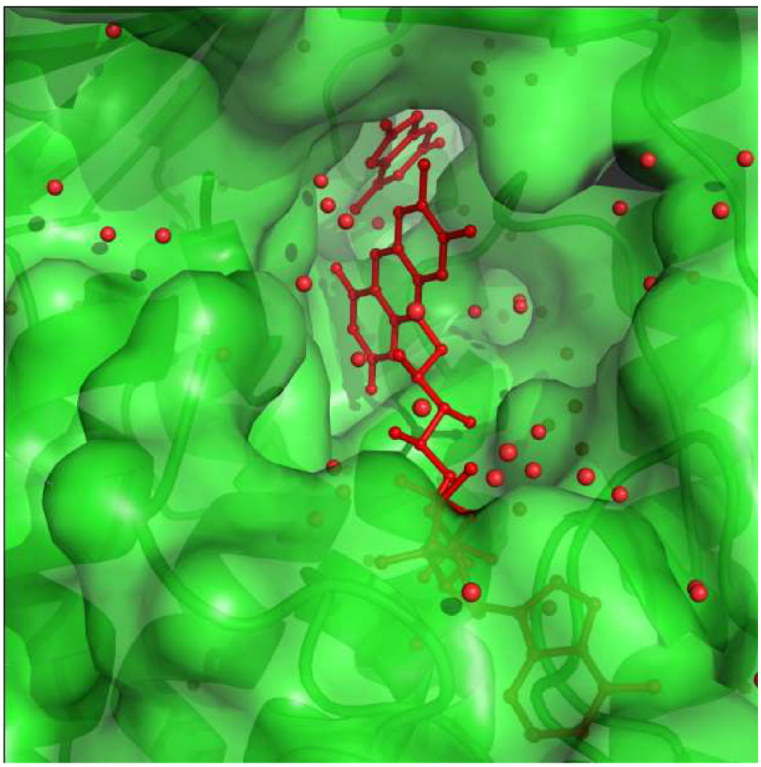

Figure 4.
Space filling model of HpxO showing the substrate tunnel leading to the active site. FAD and uric acid are red and in ball and stick. Water molecules are shown as red spheres. The surface of HpxO is colored green and the secondary structure elements are shown as cartoons.

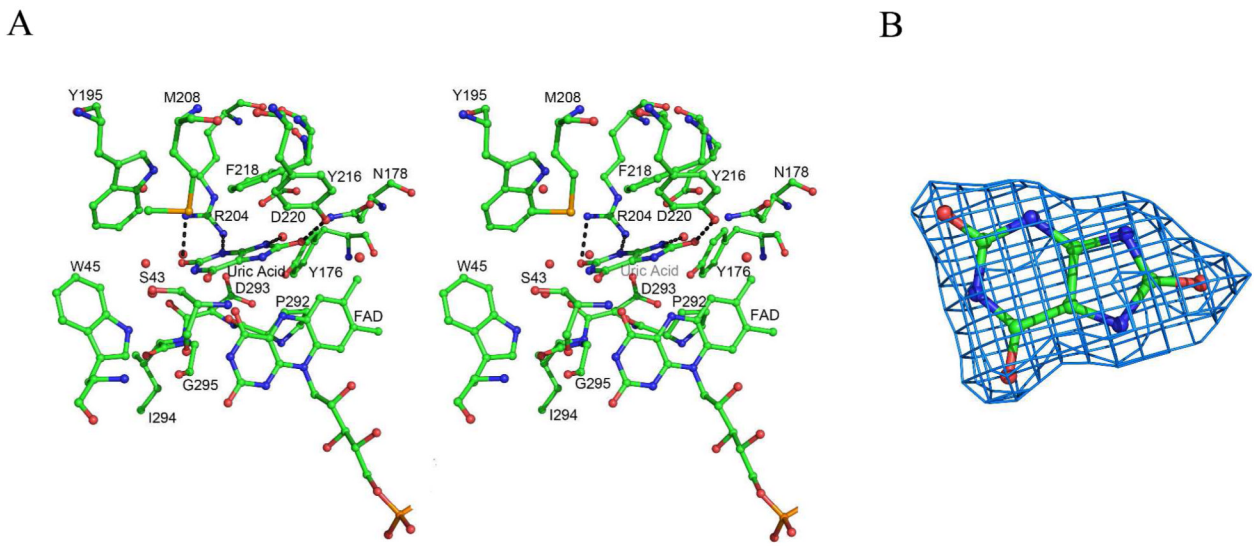

Figure 5.

Uric acid binding site. (A) Stereoview diagram of the active site of HpxO with FAD and uric acid bound. Water molecules are shown as nonbonded red spheres. Hydrogen bonds between uric acid and HpxO are shown as black, dashed lines. (B) Composite omit density is shown around the uric acid at a contour level of 3σ in blue.

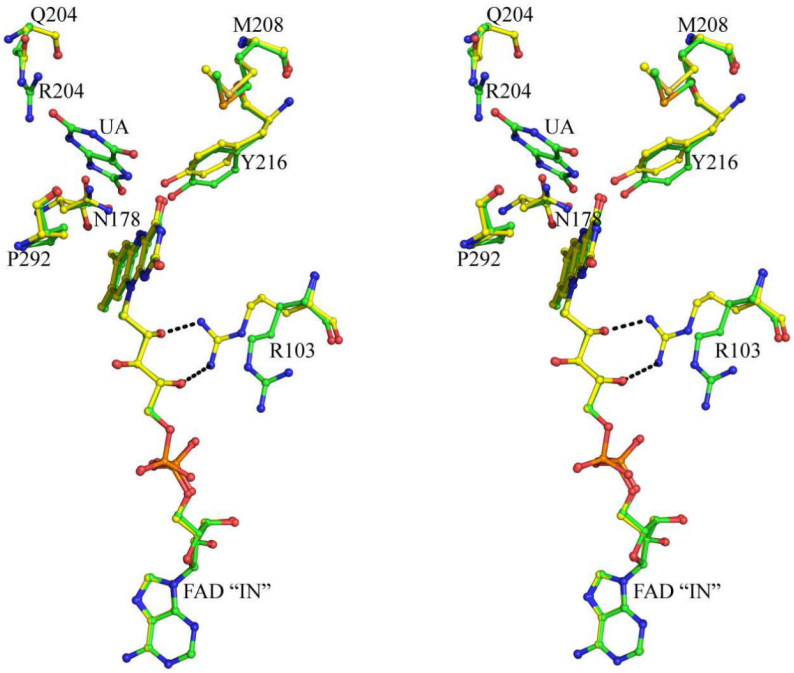

Figure 6.

Stereoview comparison of the active sites of R204Q and wild type HpxO. The carbon residues in wild type HpxO structure are shown in green and are yellow in the R204Q variant structure. Residues and ligands are shown using the ball and stick representation using the same color scheme. Interactions with the protein are indicated by black dashed lines. In the wild type structure, there is a SeMet at position 208.

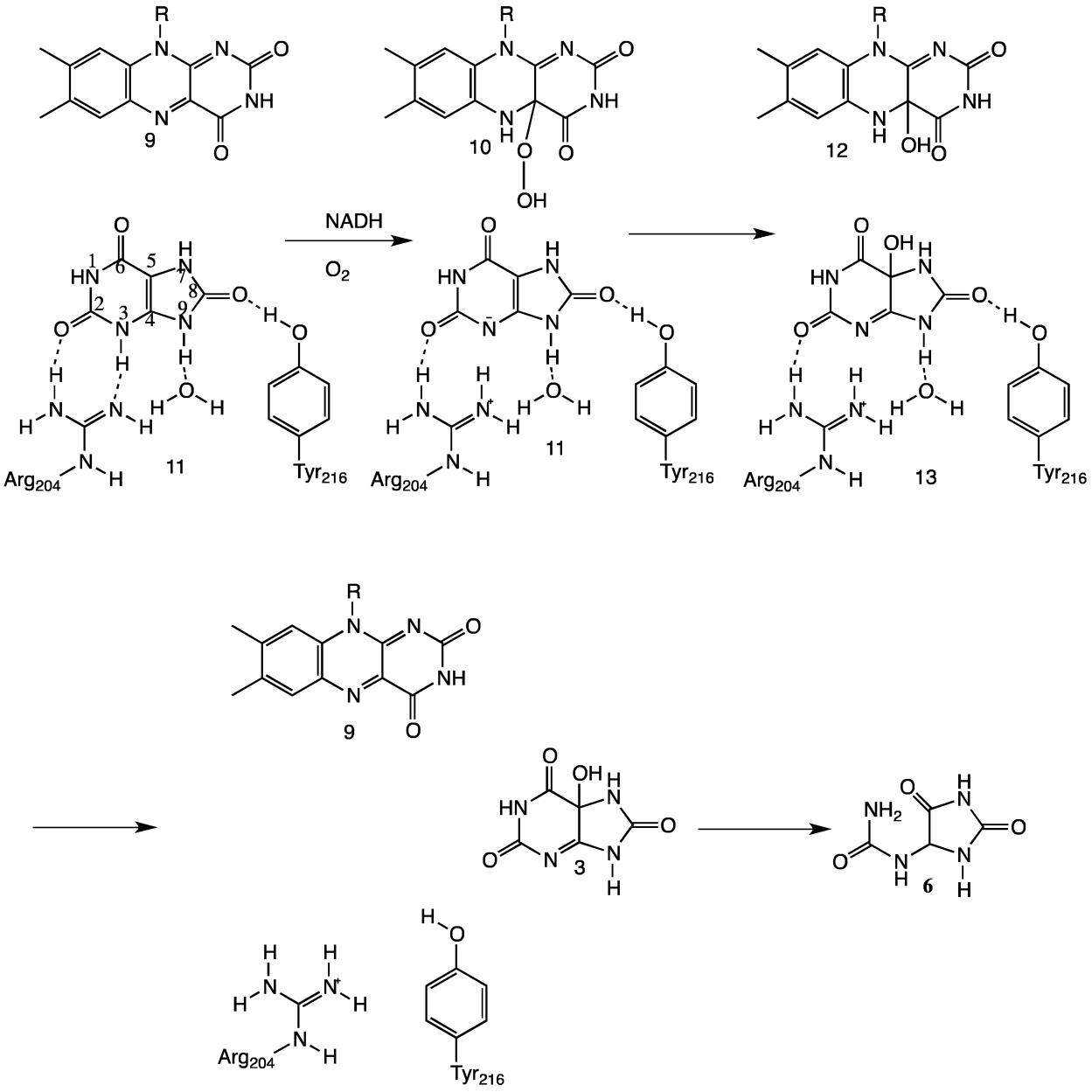

Figure 7.
Proposed mechanism for the HpxO catalyzed reaction.

Table 1

Summary of Data Collection Statistics

	SeMet HpxO	SeMetHpxO + Uric Acid	R204Q HpxO
Beamline	APS-24-IDC	APS-24-IDC	APS-24-IDC
Resolution (Å)	2.2	2.0	2.0
Wavelength (eV)	12662.0	12662.5	12662.0
Space Group	$P2_12_12_1$	$P2_12_12_1$	$P2_12_12_1$
a (Å)	66.65	67.02	67.03
b (Å)	67.65	67.84	68.77
c (Å)	82.01	82.24	81.58
Measured Reflections	157283	134891	119607
Unique reflections[a,b]	19184 (1781)	24401 (2383)	27220 (1308)
Average I/σ	22.7 (4.8)	40.9 (8.6)	27.3 (3.4)
Redundancy	8.2 (6.2)	5.6 (5.5)	4.4 (4.4)
Completeness (%)	98.4 (93.8)	99.7 (99.3)	99.4 (99.8)
Rsym[c] (%)	10.0 (27.4)	9.3 (31.1)	4.8 (37.2)

[a] Unique reflections include Bijvoet pairs.

[b] Values in parentheses are for the highest resolution shell.

[c] $R_{sym} = \Sigma\Sigma_i|I_i - \langle I \rangle| / \Sigma \langle I \rangle$, where $\langle I \rangle$ is the mean intensity of the N reflections with intensities I_i and common indices *h,k,l*.

Table 2

Summary of Data Refinement Statistics

	SeMet HpxO	SeMet HpxO + Uric Acid	R204Q HpxO
Resolution (Å)	34.9-2.20	33.9-2.04	48.0-1.97
# of protein atoms	2924	2894	2902
# of ligand atoms	53	65	54
# of water atoms	61	194	112
Reflections in working set	19144	24336	25161
Reflections in test set	974	1229	1326
Rfactor[a] (%)	20.6	19.2	19.0
Rfree[b] (%)	25.4	23.2	22.9
Rmsd from ideals			
Bonds (Å)	0.007	0.005	0.007
Angles (°)	1.029	1.035	1.082
Avg B factor (Å^2)	34.3	22.3	27.7
Ramachandran Plot			
Most favored (%)	90.7	91.0	91.6
Additionally allowed (%)	9.3	9.0	8.4
Generously allowed (%)	0	0	0
Disallowed (%)	0	0	0

[a] R factor = $\Sigma_{hkl}||F_{obs}|- k|F_{cal}||/\Sigma_{hkl}|F_{obs}|$ where F_{obs} and F_{cal} are observed and calculated structure factors, respectively.

[b] For R_{free} the sum is extended over a subset of reflections (5%) excluded from all stages of refinement.

Table 3

Kinetic Parameters for HpxO Active Site Variants.

Enzyme	k_{cat} (s^{-1})	$K_{m,\ urate}$ (μM)	$K_{m,\ NADH}$ (μM)	$k_{cat}/K_{m,\ urate}$ ($\mu M^{-1}s^{-1}$)	$k_{cat}/K_{m,\ NADH}$ ($\mu M^{-1}s^{-1}$)
WT	42 ± 2	42 ± 8	~500	1.0 ± 0.2	0.125 ± 0.030
R204Q	0.26 ± 0.006	ND	640 ± 39	ND	$\sim 10^{-4}$
Y216F	8.4 ± 0.5	90 ± 20	100 ± 35	0.093 ± 0.021	0.084 ± 0.030

ND – not determined.

Table 4

Enzymes Identified as Structurally Similar to HpxO based on DALI.

Protein	PDB ID	Z Score	RMSD	% Identical	# aligned residues
2,6-dihydroxypyridine 3-hydroxylase (DHPH)	2VOU	37.9	2.3	22	347
2-methyl-3-hydroxypyridine-5-carboxylic acid (MHPCO)	3GMC	37.6	2.6	19	339
p-hydroxybenzoate hydroxylase (PHBH)	1YKJ	34.4	3.0	15	360
Phenol hydroxylase	1FOH	31.5	2.9	16	346
3-hydroxybenzoate hydrolase (MHBH)	2DKH	21.0	3.2	16	338